Fine-Tuning Generative Models as an Inference Method for Robotic Tasks

Anonymous Author(s)
Affiliation
Address
email

Abstract: Adaptable models could greatly benefit robotic agents operating in the real world, allowing them to deal with novel and varying conditions. While approaches such as Bayesian inference are well-studied frameworks for adapting models to evidence, we build on recent advances in deep generative models which have greatly affected many areas of robotics. Harnessing modern GPU acceleration, we investigate how to quickly adapt the sample generation of neural network models to observations in robotic tasks. We propose a simple and general method that is applicable to various deep generative models and robotic environments. The key idea is to quickly fine-tune the model by fitting it to generated samples matching the observed evidence, using the cross-entropy method. We show that our method can be applied to both autoregressive models and variational autoencoders, and demonstrate its usability in object shape inference from grasping, inverse kinematics calculation, and point cloud completion.

1 Introduction

Humans and other animals maintain powerful mental models of the world [1] for navigation, object manipulation, social interaction and other day-to-day tasks. These mental models are imperfect and tend to be inaccurate. However, they are highly adaptable and are frequently updated upon arrival of new information. Robotic agents operating in diverse and unstructured environments may also be required to adjust their behavior, and would therefore benefit from adaptable models similar to the ones humans hold. Recent studies in robot manipulation and navigation have focused on scenarios where an accurate model can be learned and used as-is in downstream planning tasks [2, 3, 4]. In contrast, inspired by biological mental models, this paper focuses on how to efficiently adapt a model to novel information.

Natural approaches to updating models given new evidence such as *Bayesian inference* have been used extensively in computer vision and robotics [5, 6]. When the modelled probability distributions are low-dimensional, Bayesian inference may have closed form solutions or the posterior can be numerically estimated using methods such as Markov chain Monte Carlo (MCMC, [7]). However, there is growing interest in using high-dimensional *deep generative models* for robotics, which can represent complex and diverse data. Advances such as *variational autoencoders* [8] and *diffusion models* [9] make it possible to learn diverse and high-dimensional distributions. For such expressive models, Bayesian inference techniques are not suitable, and they cannot operate on the time-scale required for robotic tasks [10]. Another approach, which has been found effective with deep generative models, is to *train* them to adapt by conditioning on possible observations [11, 12]. However, this paradigm may fall short when faced with out-of-distribution evidence at test-time.

We propose a simple approach for updating the parameters of deep generative models given empirical observations, to approximate complex posterior distributions. Our method requires a forward simulation of the environment which can produce observations given a model, and a similarity function for observations. We build on GPU-based physics simulation [13] and model training to perform

Submitted to the 7th Conference on Robot Learning (CoRL 2023). Do not distribute.

fast inference in a novel robotic scenario by fine-tuning the generative model weights. Considering the parametric nature of deep generative models, we use a version of the cross-entropy method (CEM [14]) to quickly update the parameters to generate observations conforming with the available evidence. We dub our method MACE, for **M**odel **A**daptation with the **C**ross-**E**ntropy method.

To showcase MACE, we focus on robotic domains where the forward simulation step is easily performed using off-the-shelf physical simulators. We demonstrate the versatility of MACE on several robotic manipulation tasks that we frame as model adaptation, using two different types of deep generative models. In particular, we demonstrate results on object identification from position measurements of a multi-fingered robot gripper, on recovery of object point clouds given partial measurements (as generated by depth sensors) and on an inverse kinematics (IK) task in the presence of obstacles. In all of these environments, the posterior has a rich multi-modal structure. We demonstrate that MACE is indeed capable of producing diverse posterior samples for a variety of observations, and that it outperforms baseline approaches in diversity and accuracy. In terms of speed, we show that by exploiting GPU-based simulation and inference, our fine-tuning can be preformed online in a competitive time frame. For example, in the IK tasks, we find that MACE can outperform the MoveIt [15] library in quickly finding IK solutions for complex scenarios.

2 Related Work

Bayesian inference is concerned with computing the posterior distribution of the model given observations. Exact computation is possible for simple models that admit conjugate priors, and Markov chain Monte Carlo (MCMC) can be used for general models [7]. Approximate Bayesian computation (ABC [16]) allows sampling from the posterior without an exact likelihood, but with some similarity function between observations. MACE is inspired by these approaches, and expedites the search for better samples using the cross-entropy method (CEM [14]). Recent work by Engel et al. [17] introduces a Bayesian model update scheme using CEM which is related to ours. However, Engel et al. [17] require the true likelihood, and their method is limited to relatively small models, while ours can be applied to deep generative models.

Bayesian inference has been used extensively in robotics in the context of state estimation, localization, and mapping [5, 18]. In recent work, Marlier et al. [19] use Bayesian estimation of a posterior distribution of grasp poses for multi-finger object grasping, and Pastor et al. [10] use Bayesian inference with LSTM [20] to classify objects using tactile sensors. Both the above are application-specific, while MACE is a general approach applicable to a variety tasks and generative models.

Another approach is to amortize inference by learning an approximate posterior using data from the joint distribution $p(\boldsymbol{x}, \boldsymbol{o})$ such as in the *conditional variational autoencoder* (CVAE) model [21]. We compare MACE with a CVAE baseline, and show that while our inference procedure is slower, MACE produces a more diverse posterior. Furthermore, since MACE leverages a similarity function between observations, it can work for observations that are out of distribution with respect to $p(\boldsymbol{x}, \boldsymbol{o})$, unlike the CVAE. Finally, MACE can tune the same prior model with different modalities of observations without retraining.

Meta-learning, and *meta-RL* in particular, is an alternative approach to quickly adapt behavior to new evidence [22]. However, meta-RL is typically model-free, and learns how to adapt a policy [22, 23]. Model-based meta-RL approaches such as Zintgraf et al. [12] use a CVAE to condition on the history of observations. Whether such methods could be improved using our inference method is an interesting direction for future research.

3 Model Adaptation with the Cross-Entropy Method

We now describe MACE, our method for adapting deep generative models to environment observations using the cross-entropy method. We begin by describing the setup and the types of tasks we aim to solve; next, we discuss our update rule and present the full algorithm.

3.1 Problem Formulation

In the robotics context, an *inference problem* involves the recovery of *task* parameters given observations of the environment. We assume some distribution $p(\boldsymbol{x})$ over task representations $\boldsymbol{x} \in \mathcal{X}$. A task description $\boldsymbol{x}$ could be a point cloud (PC) of an object as in a grasping task; an image input for more complex manipulation; or a desired joint configuration in a reaching task. MACE requires access to a generative model representing a parametric distribution over task representations $p(\boldsymbol{x}; \theta)$. We assume the generative model is initially trained to represent the prior, i.e., for some initial parameter θ_0 it holds that $p(\boldsymbol{x}; \theta_0) = p(\boldsymbol{x})$.

Although the task representation $\boldsymbol{x}$ is unknown, some information about it can be observed. We denote this information $\boldsymbol{o} \in \mathcal{O}$ (for *observation*) and note that it can be of any form, For example, in a grasping task, $\boldsymbol{o}$ could be a partial PC obtained from a depth sensor (while $\boldsymbol{x}$ is the full object model); in a reaching task, $\boldsymbol{o}$ could represent obstacles for the robot to avoid.

A central component of MACE is a *simulator* of the task. Exact environment simulators are often hard to design, leaving gaps to the reality they attempt to simulate [18]. However, for our purposes, we only require the simulator to emit observations of a similar modality to the ones emitted by the environment. Therefore, the simulator can be viewed as a probability distribution $\hat{p}(\boldsymbol{o}|\boldsymbol{x})$, providing observations given task representations.

The goal of the inference task is to train the parametric model $p(\boldsymbol{x}; \boldsymbol{\theta})$ to produce a distribution closely resembling the posterior $p(\boldsymbol{x}|\boldsymbol{o})$.

3.2 Updating the Model

We aim to update the model parameters $\boldsymbol{\theta}$ so that the generative model $p(\boldsymbol{x}; \boldsymbol{\theta})$ more closely resembles the posterior $p(\boldsymbol{x}|\boldsymbol{o})$. We can do this by minimizing the Kullback-Leibler (KL) divergence between the posterior and the parametric model:

$$\arg\min_{\boldsymbol{\theta}} D_{\mathrm{KL}}\left(p(\boldsymbol{x}|\boldsymbol{o}) \| p(\boldsymbol{x}; \boldsymbol{\theta})\right) = \arg\min_{\boldsymbol{\theta}} \int p(\boldsymbol{x}|\boldsymbol{o}) \log p(\boldsymbol{x}|\boldsymbol{o}) d\boldsymbol{x} - \int p(\boldsymbol{x}|\boldsymbol{o}) \log p(\boldsymbol{x}; \boldsymbol{\theta}) d\boldsymbol{x}.$$

The parametric model is only present in the second term, therefore we can maximize it to minimize the entire KL divergence. Since the posterior $p(\boldsymbol{x}|\boldsymbol{o})$ is unknown, we use Bayes' rule to replace it with the likelihood $p(\boldsymbol{o}|\boldsymbol{x})$: $\arg\max_{\boldsymbol{\theta}} \int p(\boldsymbol{x}|\boldsymbol{o}) \log p(\boldsymbol{x}; \boldsymbol{\theta}) d\boldsymbol{x} = \arg\max_{\boldsymbol{\theta}} \int \frac{p(\boldsymbol{o}|\boldsymbol{x}) p(\boldsymbol{x})}{p(\boldsymbol{o})} \log p(\boldsymbol{x}; \boldsymbol{\theta}) d\boldsymbol{x} = \arg\max_{\boldsymbol{\theta}} \mathbb{E}_{\boldsymbol{x} \sim p(\boldsymbol{x})} \left[p(\boldsymbol{o}|\boldsymbol{x}) \log p(\boldsymbol{x}; \boldsymbol{\theta})\right]$.

The likelihood of the observation $p(\boldsymbol{o}|\boldsymbol{x})$ is also an unknown quantity. However, we may estimate it using the forward simulator, which can produce observations $\boldsymbol{o}$ given $\boldsymbol{x}$. We define a *score function* as any function $S : \mathcal{O} \times \mathcal{O} \to [0, 1]$ indicating similarity between pairs of observations, and assume $\mathbb{E}_{\boldsymbol{o}' \sim \hat{p}(\boldsymbol{o}|\boldsymbol{x})} S(\boldsymbol{o}', \boldsymbol{o})$ is an estimate of $p(\boldsymbol{o}|\boldsymbol{x})$. An intuitive case to justify this assumption is when observations $\boldsymbol{o}$ are discrete, and $S(\boldsymbol{o}', \boldsymbol{o}) = \mathbf{1}_{\mathrm{o}'=\mathrm{o}}$ is an indicator of whether $\boldsymbol{o}'$ is equal to the evidence $\boldsymbol{o}$ [1]. In practice, as our simulators are deterministic, we replace the expectation with a single observation $\boldsymbol{o}'$ per sample $\boldsymbol{x}$. In the following, we abuse notation by referring to $\mathbb{E}_{\boldsymbol{o}' \sim \hat{p}(\boldsymbol{o}|\boldsymbol{x})} S(\boldsymbol{o}', \boldsymbol{o})$ as $S(\boldsymbol{o}', \boldsymbol{o})$. Plugging in the score function, the optimization problem becomes:

$$\arg\max_{\boldsymbol{\theta}} \mathbb{E}_{\boldsymbol{x} \sim p(\boldsymbol{x})} \left[S(\boldsymbol{o}', \boldsymbol{o}) \log p(\boldsymbol{x}; \boldsymbol{\theta})\right]. \tag{1}$$

Recalling our assumption that $p(\boldsymbol{x}; \boldsymbol{\theta}_0) = p(\boldsymbol{x})$, Eq. 1 can be optimized using importance sampling: $\arg\max_{\boldsymbol{\theta}} \frac{1}{N} \sum_{i=1}^{N} \frac{p(\boldsymbol{x}; \boldsymbol{\theta}_0)}{p(\boldsymbol{x}; \boldsymbol{\theta})} S(\boldsymbol{o}_i, \boldsymbol{o}) \log p(\boldsymbol{x}_i; \boldsymbol{\theta})$, where $\boldsymbol{x}_i \sim p(\boldsymbol{x}; \boldsymbol{\theta})$, the sampling distribution. One question, however, is how to choose an effective sampling distribution which places enough mass on high-scoring $\boldsymbol{x}$ values. Inspired by the iterative approach of Engel et al. [17], we optimize this objective iteratively using stochastic gradient descent. At each iteration, we use the parametric model from the previous iteration as the sampling distribution and take a few gradient

[1] For other examples of score functions, see the environment descriptions in Sec. 4.

steps to obtain the next model parameters. The objective at iteration t is given by:

$$\arg\max_{\boldsymbol{\theta}} \frac{1}{N} \sum_{i=1}^{N} \frac{p(\boldsymbol{x};\boldsymbol{\theta}_0)}{p(\boldsymbol{x};\boldsymbol{\theta}_{t-1})} S(\boldsymbol{o}_i, \boldsymbol{o}) \log p(\boldsymbol{x}_i;\boldsymbol{\theta}), \tag{2}$$

with $x_i \sim p(\boldsymbol{x};\boldsymbol{\theta}_{t-1})$. In practice, we find that the importance sampling term in this objective makes it difficult to optimize due to large discrepancies between the parametric distributions[2]. Instead, we introduce another approximation and remove the importance sampling term $\frac{p(\boldsymbol{x})}{p(\boldsymbol{x};\boldsymbol{\theta})}$ from Eq. 2.

To further improve performance and shorten training times, we follow the cross-entropy method (CEM) formulation described by Botev et al. [24]. We view the objective in Eq. 1 as the problem of finding a distribution $p(\boldsymbol{x};\boldsymbol{\theta})$ which produces samples with high scores $S(\boldsymbol{o}', \boldsymbol{o})$. To optimize $S(\boldsymbol{o}', \boldsymbol{o})$ (which is implicitly a function of $\boldsymbol{x}$ through the simulator), we treat $p(\boldsymbol{x};\boldsymbol{\theta})$ as an importance sampling distribution and adjust it such that it samples values of $\boldsymbol{x}$ that are close to the ones implicitly maximizing $S(\boldsymbol{o}', \boldsymbol{o})$. At each iteration t we sample a batch $\{\boldsymbol{x}_i \sim p(\boldsymbol{x};\boldsymbol{\theta}_{t-1})\}_{i=1}^{N}$, obtain observations using the simulator $\{\boldsymbol{o}_i \sim \hat{p}(\boldsymbol{o}|\boldsymbol{x}_i)\}_{i=1}^{N}$ and calculate their respective scores $\{S(\boldsymbol{o}_i, \boldsymbol{o})\}_{i=1}^{N}$. The top qN samples with the best scores are selected, where q is a pre-selected quantile hyperparameter. We define $\delta = S(\boldsymbol{o}_{\lfloor qN \rfloor}, \boldsymbol{o})$, the score function value for the $\lfloor qN \rfloor$-th sample. The complete CEM-inspired MACE objective is given by:

Algorithm 1: MACE (**M**odel **A**daptation with the **C**ross-**E**ntropy method)

Input: Prior model $p(\boldsymbol{x};\boldsymbol{\theta}_0)$, simulator $\hat{p}(\boldsymbol{o}|\boldsymbol{x})$, observation $\boldsymbol{o}$, quantile parameter q, gradient steps parameter M

for $t \leftarrow 1, \ldots, T$ **do**
- Sample $\boldsymbol{x}_1, \ldots, \boldsymbol{x}_N \sim p(\boldsymbol{x};\boldsymbol{\theta}_{t-1})$
- Obtain $\boldsymbol{o}_1, \ldots, \boldsymbol{o}_N \sim \hat{p}(\boldsymbol{o}|\boldsymbol{x})$ using the simulator
- Calculate $S(\boldsymbol{o}_i, \boldsymbol{o})$ for all $\boldsymbol{o}_1, \ldots, \boldsymbol{o}_N$
- Select top qN samples, set $\delta = S(\boldsymbol{o}_{\lfloor qN \rfloor}, \boldsymbol{o})$
- Optimize $\arg\max_{\boldsymbol{\theta}} \sum_{i=1}^{N} \mathbf{1}_{S(\boldsymbol{o}_i,\boldsymbol{o}) \geq \delta} \log p(\boldsymbol{x};\boldsymbol{\theta}_t)$ using M steps of SGD

return updated model $p(\boldsymbol{x};\boldsymbol{\theta}_T)$

$$\arg\max_{\boldsymbol{\theta}} \sum_{i=1}^{N} \mathbf{1}_{S(\boldsymbol{o}_i,\boldsymbol{o}) \geq \delta} \log p(\boldsymbol{x}_i;\boldsymbol{\theta}). \tag{3}$$

Botev et al. [24] solve a stochastic program for the each iteration of $\boldsymbol{\theta}$. Instead, we optimize this objective via stochastic gradient descent (SGD) as described above. The full MACE algorithm is shown in Alg. 1.

3.2.1 Implementation

Although MACE is suitable in principle for any generative model, some considerations must be made for specific types of models.

Autoregressive models provide an explicit likelihood value for a sample $\boldsymbol{x}$ using the chain rule: $p(\boldsymbol{x}) = \prod_i p(x_i|x_{i-1}, \ldots, x_0)$. Therefore, they are straightforward to use with MACE by denoting the model weights as $\boldsymbol{\theta}$ and directly optimizing the objective in Eq. 3.

VAEs do not provide an explicit likelihood value $p(\boldsymbol{x})$. However, they are trained with a lower bound estimate of $p(\boldsymbol{x})$, namely the Evidence Lower Bound (ELBO) $\log p(\boldsymbol{x}|\boldsymbol{z};\boldsymbol{\psi}) - D_{\mathrm{KL}}\left(q(\boldsymbol{z}|\boldsymbol{x};\boldsymbol{\phi}) \| p(\boldsymbol{z})\right)$, where $p(\boldsymbol{x}|\boldsymbol{z};\boldsymbol{\psi})$ is the VAE decoder parameterized by $\boldsymbol{\psi}$, $q(\boldsymbol{z}|\boldsymbol{x};\boldsymbol{\phi})$ is the encoder parameterized by $\boldsymbol{\phi}$ and $p(\boldsymbol{z})$ is the prior distribution of the latent space parameterized by $\boldsymbol{\mu_z}, \boldsymbol{\sigma_z}$. We can use the ELBO in Eq. 3 as a lower bound of the log-likelihood term $\log p(\boldsymbol{x};\boldsymbol{\theta})$, optimizing the VAE parameters: $\arg\max_{\boldsymbol{\psi},\boldsymbol{\phi}} \sum_{i=1}^{N} \mathbf{1}_{S(\boldsymbol{o}_i,\boldsymbol{o}) \geq \delta} \left[\log p(\boldsymbol{x}_i|\boldsymbol{z}_i;\boldsymbol{\psi}) - D_{\mathrm{KL}}\left(q(\boldsymbol{z}_i|\boldsymbol{x}_i;\boldsymbol{\phi}) \| p(\boldsymbol{z})\right)\right]$. We found the optimization of the entire set of VAE weights $\boldsymbol{\psi}, \boldsymbol{\phi}$ to be difficult. Instead, we use $\boldsymbol{\theta} = \{\boldsymbol{\mu_z}, \boldsymbol{\sigma_z}\}$ as our tuned parameters, and keep the encoder and decoder weights frozen. This choice of $\boldsymbol{\theta}$ only affects the

[2] We compare MACE to this objective as a baseline; see experiment results in Sec. 4.1 and Sec. 4.2

second term of the objective, and specifically $p(\boldsymbol{z})$. The objective of this version of MACE, which we dub MACE-VAE, then becomes: $\arg\max_{\boldsymbol{\theta}} \sum_{i=1}^{N} \mathbf{1}_{S(\boldsymbol{o}_i,\boldsymbol{o})\geq\delta} \left[-D_{\mathrm{KL}}\left(q(\boldsymbol{z}_i|\boldsymbol{x}_i)\|p(\boldsymbol{z};\boldsymbol{\theta})\right)\right]$.

4 Experiments

MACE is designed to allow deep generative models to adapt quickly to new evidence. To demonstrate the potential of MACE in robotic applications, we consider several domains in which these models are used to capture complex data distributions and show that MACE leads to practical solutions, improving on the alternatives. In the subsections below, we describe two of these environments and how they fit our setting, followed by a summary of experiment results. A third environment, in which we use MACE to recover object point clouds from partial point cloud observations, is described in Appendix C, due to lack of space.

4.1 Inferring Object Shapes by Grasping

Inferring object shapes from tactile measurements [10] is vital when visual sensors are unavailable or limited. We investigate whether details about an object can be inferred using only the contact points between it and the robot gripper fingertips. Differing from the approach of Pastor et al. [10], which aims to classify objects into 36 classes, we consider an expressive prior distribution over possible shapes represented by a deep generative model.

Dataset. We use the "airplane" class from the ShapeNet [25] dataset as a representative collection of objects with complex shapes. This class contains 4045 objects, represented as 2048-point PCs.

Model. The prior generative model $p(\boldsymbol{x};\boldsymbol{\theta}_0)$ is a VAE trained on full PCs of objects. We use MACE-VAE as described in Sec. 3.2.1. Our VAE architecture uses PointNet [26] in the encoder and a fully connected decoder, and is based on the implementation used in Daniel and Tamar [27]. Additional training details and hyperparameters can be found in Appendix A.

Simulator. For ease of implementation, we use a simple geometric simulator to calculate contact points. Details can be found in Appendix A.

Score Function. The score function for k-fingered grasps, aggregating distances between contact points and clipped to the range of $[0, 1]$, is defined as $S(\boldsymbol{o}', \boldsymbol{o}) = \max\left(1 - \frac{1}{k}\sum_{j=1}^{k} ||p_j^{(\boldsymbol{o}')} - p_j^{(\boldsymbol{o})}||, 0\right)$, where $p_j^{(\boldsymbol{o})}$ is the j-th contact point of observation $\boldsymbol{o}$.

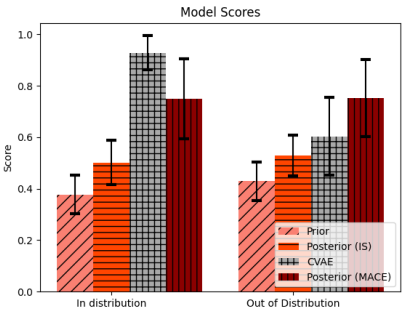

(a) Average scores

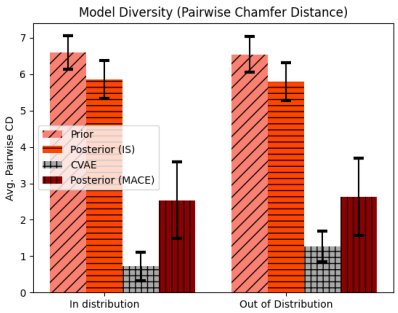

(b) Sample diversity

Figure 1: Quantitative results for the multi-fingered grasping experiments.

Inferring Object Shapes by Grasping: Results

We adapt the distribution of airplane models by obtaining a single observation $\boldsymbol{o}$ representing contact points of $k = 5$ robot fingers with an unknown object. To evaluate the tuning process, we sample 49 objects $\boldsymbol{x}_i$ from the prior and another 49 from the posterior, and calculate the average score for the matching observations $\boldsymbol{o}_i$ obtained from the simulator using $S(\boldsymbol{o}_i, \boldsymbol{o})$. In addition, we compute the pairwise Chamfer distances between every two objects in each sampled set and take their mean as a measure of sample diversity. Scores and sample diversity are presented in Fig. 1.

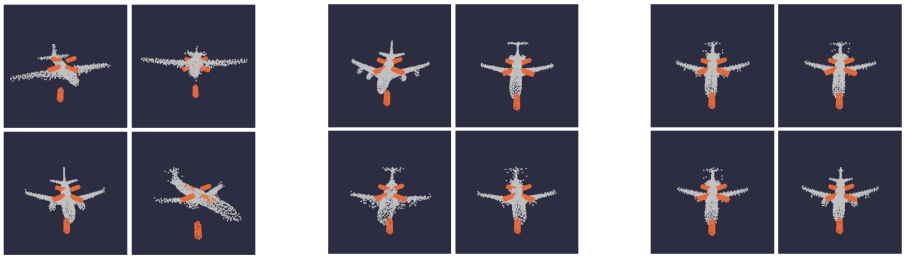

(a) Samples from the prior (b) Samples from the posterior (c) Samples from the CVAE

Figure 2: Tuning for the multi-finger grasping domain. Model samples are shown in white and finger positions and contact points of the given observation $\boldsymbol{o}$ are represented by orange cylinders.

As a baseline, we conduct the same experiment using the importance sampling loss described in Eq. 2. We replace the log-likelihood term with the ELBO as in MACE-VAE (see Sec. 3.2.1), with the rest of the algorithm components as in Alg. 1. We find that this objective performs poorly compared to MACE (see Fig. 1). Moreover, optimizing it is an order of magnitude (up to $20\times$) slower than using MACE.

As an additional baseline, we train a CVAE conditioned on contact points calculated by grasping each training-set object in simulation. Albeit its advantage of fast amortized inference, the CVAE is limited to observations seen in its training set. We demonstrate this disadvantage in the out-of-distribution experiment below. We tune our model and compare results to the CVAE baseline using 100 objects from the held-out test set of the ShapeNet "airplane" class, all with the same observation $\boldsymbol{o}$, in which the robot finger directions are the four diagonal corners of the xy plane, and a fifth along the x axis. Quantitative results can be seen in Fig. 1. The CVAE baseline outperforms the tuned posterior in scores, but produces a distribution with lower diversity.

In addition to the quantitative results, we present samples from the prior, posterior and CVAE models in Fig. 2 . These showcase the diversity of the model tuned by MACE compared to the CVAE distribution. Additional samples and tuning hyperparameters can be found in Appendix A.

Out-of-distribution experiment. We run the entire set of experiments a second time using a different observation, with the fifth finger pointing along the opposite direction of the x axis. This is out of the joint distribution $p(\boldsymbol{x}, \boldsymbol{o})$ which the CVAE baseline was trained on. Consequently, its results greatly deteriorate. Conversely, the model tuned by MACE outperforms it both in diversity and in scores. Results can be seen in Fig. 1. Visuals of samples from the CVAE and the MACE-tuned posterior model with the new OOD observation can be viewed in Fig. 4 in Appendix A.

4.2 Inverse Kinematics with Obstacles

Inverse kinematics (IK) is the calculation of the configuration of robot joints given a desired pose in Cartesian space. IK calculation is an especially challenging optimization problem when obstacles are involved and has no closed-form solution in the general case. While previous work has attempted to learn IK using generative models [28, 29, 30], we focus on tuning a pre-trained IK model to consider novel obstacles. We view the obstacle-constrained IK problem as an inference problem, where the prior $p(\boldsymbol{x}; \boldsymbol{\theta}_0)$ is a generative model trained to represent a distribution of joint configurations conditioned on the end-effector position[3] when no obstacles are present. Note that this is a complex and multi-modal distribution which accounts both for self-collisions and for the conditioning on the desired pose. The observation is an obstacle configuration, and the posterior captures a distribution over non-colliding joint configurations.

Dataset. We collect 10M random valid configurations of a Franka Emika Panda 7-DoF robotic manipulator using PyBullet physics simulation [31], and record their matching end-effector positions.

[3]The pose can also include the end-effector orientation; in this work we focus on position-only IK.

We collect these configurations in an environment with no obstacles present; therefore, valid configurations are ones which conform to the joint limits of the robot, and where the robot is not in collision with itself.

Model. We train an autoregressive model with joint positions generated sequentially, conditioned on the previous joints as well as the end-effector position: $p(q_1|\boldsymbol{p}_{ee})$, $p(q_2|q_1, \boldsymbol{p}_{ee})$ etc. Probability distributions for each joint are represented by Gaussian mixture models. Further architecture and training details can be found in Appendix B.

Simulator. We use open-source physical simulation environments, optionally with obstacles in the robot workspace. The simulated robot can be set to a specific joint configuration $\boldsymbol{q}$. The simulator returns whether the robot is in collision with itself or the obstacles, as well as the distance between the desired position and the actual end-effector position obtained by setting the robot to $\boldsymbol{q}$.

Score Function. We opt for a score function that penalizes collisions harshly, and therefore set $S(\boldsymbol{o}', \boldsymbol{o}) = 0$ if the robot is in collision in a given configuration. Otherwise, the score is proportional to the distance between the generated end-effector position and the desired position: $S(\boldsymbol{o}', \boldsymbol{o}) = \exp(-||\boldsymbol{p}_{ee,\text{desired}} - \boldsymbol{p}_{ee,\text{actual}}||)$.

Inverse Kinematics with Obstacles: Results

We run two experiments in this domain, with different types of obstacle in the workspace, both using the PyBullet simulation environment [31]. In the first experiment, the obstacle is a vertical window, with the desired end-effector positions located beyond it. A qualitative sample from the prior model $p(\boldsymbol{x}; \boldsymbol{\theta}_0)$ (trained with no obstacles) can be viewed in Fig. 3a, where it is clear that many of the sampled configurations are in collision with the obstacle. Fig. 3b shows samples from the posterior model tuned with MACE, which almost never collide with the obstacle.

To show that the result does not depend on obstacle shape, we conduct a similar experiment with a wall obstacle, with the target end-effector position behind it. Samples from the model tuned by MACE can be seen in Fig. 3c, again diverse and non-colliding. We verify this result quantitatively by sampling 10 goal end-effector positions behind the wall, and tuning the model with the respective score functions. As a baseline, we also tune the model with the importance sampling (IS) objective of Eq. 2. We report the mean scores over 1000 samples from the prior, the posterior tuned with MACE and the posterior tuned with the IS baseline in Table 1. We additionally report the success rate, calculated as the percentage of sampled configurations which are not in a collision state. The results clearly show improvement when tuning with MACE. Tuning hyperparameters and additional samples can be found in Appendix B.

Table 1: Inverse Kinematics Results

Model	Score	Success Rate
Prior	0.129 ± 0.015	0.132 ± 0.015
Posterior (MACE)	0.937 ± 0.079	0.941 ± 0.079
Posterior (IS)	0.317 ± 0.121	0.339 ± 0.122

Comparison to MoveIt Inverse Kinematics

The MoveIt [15] motion planning framework included with ROS has a standard IK service, used to infer goal positions for motion planning algorithms. While it is a powerful tool, we demonstrate that MACE can improve on its solutions where it struggles to find them quickly. We construct a scenario of a box in front of the robot, with the desired end-effector position inside it (see Fig. 3d). Using our prior model only (no tuning steps, for maximal speed), we sample 20 batches and test them for collisions in the IsaacGym [13] GPU-based simulator, using our score function. We take the configurations with the maximum score as our IK solution. In Table 2, we report calculation time as well as solution accuracy for our method compared to MoveIt. In addition, since MoveIt depends on the initial robot position for the IK calculation, we use the position sampled from our model as an initial position for MoveIt, thus reaping the benefits of both methods. Time and accuracy for this setting are reported in the third column of Table 2. Experiment details (including a MACE adaptation experiment for the box domain) and additional visual results are available in Appendix B.

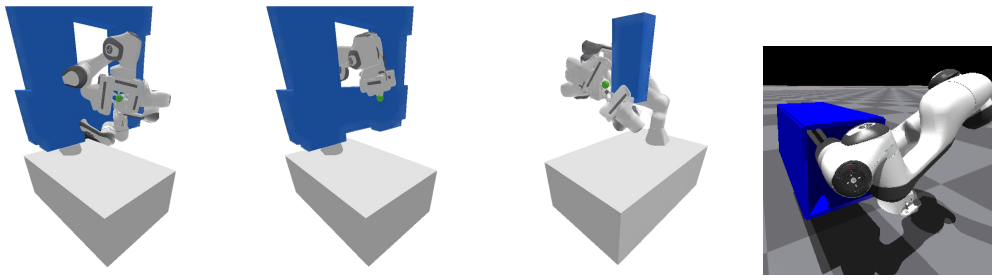

(a) Window task: prior (b) Window task: tuned (c) Wall task: tuned (d) Box task

Figure 3: Tuning for the robot inverse kinematics domain. The obstacle is shown in blue, while the goal end-effector position is shown by a green ball. While Fig. 3a shows the prior distribution overlayed with the window obstacle, the same prior was used for all tasks (conditioned on the appropriate end-effector targets). Fig. 3b displays samples from the posterior distribution tuned with MACE for the window obstacle, while Fig. 3c shows the same for the wall obstacle. In both cases, the posterior rarely admits configurations colliding with the obstacles, while remaining diverse.

Table 2: Inverse Kinematics Comparison to MoveIt for the Box Task

MACE		**MoveIt**		**MACE + MoveIt**	
Time (s)	Acc. (cm)	Time (s)	Acc. (cm)	Time (s)	Acc. (cm)
0.106 ± 0.008	1.92 ± 3.01	1.553 ± 1.103	$< 10^{-5}$	0.641 ± 0.925	$< 10^{-5}$

5 Limitations

Forward simulator. A simulator that emits observations similar to the environment may not always be available, causing a sim-to-real gap which may deteriorate results. Approaches such as domain randomization [32, 18] may mitigate this problem.

Inference speed. In our experiments, MACE inference takes between $7-65$ seconds (depending on the domain) which is still not fast enough for real-time inference applications. While the sequential nature of MACE optimization is an unavoidable computational limitation, code optimizations as well as faster hardware[4] could dramatically speed up computation.

Quality of the prior. The quality of the tuned posterior depends greatly on the quality of the pre-trained deep generative model: if high-scoring samples have low probability under the prior, MACE may not find them. In our experiments, we found that deep generative models provide priors accurate enough for the domains we investigated.

6 Conclusion and Outlook

We presented MACE, a method for adapting deep generative models using the cross-entropy method, and demonstrated its usage for multiple robotic tasks. MACE allows the model to quickly adapt to previously unseen conditions while producing diverse posterior distributions. Our promising results for inverse kinematics show that deep generative models, when tuned appropriately using MACE, may help speed up robotic problems that are typically solved using non-learning based approaches.

In future work, we intend to explore ways to expedite the optimization process and improve the usability of MACE in robotic tasks. Additionally, in this work we only considered the inference problem. However, in a realistic scenario the agent may also have control over *which observations to acquire*. In this case, it would be interesting to extend MACE to an active sampling method. Another related direction is to use MACE as an inference method for meta-RL, replacing the currently dominating CVAE-based approaches [12, 34].

[4] our experiments used unoptimized PyTorch [33] code and a single Nvidia GTX 1080 Ti GPU

References

[1] P. N. Johnson-Laird. Mental models and human reasoning. *Proceedings of the National Academy of Sciences*, 107(43):18243–18250, 2010.

[2] J. Redmon and A. Angelova. Real-time grasp detection using convolutional neural networks. In *2015 IEEE international conference on robotics and automation (ICRA)*, pages 1316–1322. IEEE, 2015.

[3] A. Nagabandi, G. Kahn, R. S. Fearing, and S. Levine. Neural network dynamics for model-based deep reinforcement learning with model-free fine-tuning. In *2018 IEEE international conference on robotics and automation (ICRA)*, pages 7559–7566. IEEE, 2018.

[4] D. Kalashnikov, A. Irpan, P. Pastor, J. Ibarz, A. Herzog, E. Jang, D. Quillen, E. Holly, M. Kalakrishnan, V. Vanhoucke, et al. Qt-opt: Scalable deep reinforcement learning for vision-based robotic manipulation. *arXiv preprint arXiv:1806.10293*, 2018.

[5] S. Thrun, W. Burgard, and D. Fox. *Probabilistic Robotics*. MIT Press, 2005.

[6] R. Szeliski. *Computer vision: algorithms and applications*. Springer Nature, 2022.

[7] D. Barber. *Bayesian reasoning and machine learning*. Cambridge University Press, 2012.

[8] D. P. Kingma and M. Welling. Auto-encoding variational bayes. In *International conference on LEarning representations*, 2013.

[9] J. Ho, A. Jain, and P. Abbeel. Denoising diffusion probabilistic models. *Advances in Neural Information Processing Systems*, 33:6840–6851, 2020.

[10] F. Pastor, J. García-González, J. M. Gandarias, D. Medina, P. Closas, A. J. García-Cerezo, and J. M. Gómez-de Gabriel. Bayesian and neural inference on lstm-based object recognition from tactile and kinesthetic information. *IEEE Robotics and Automation Letters*, 6(1):231–238, 2020.

[11] W. Yu, J. Tan, C. K. Liu, and G. Turk. Preparing for the unknown: Learning a universal policy with online system identification. *arXiv preprint arXiv:1702.02453*, 2017.

[12] L. Zintgraf, K. Shiarlis, M. Igl, S. Schulze, Y. Gal, K. Hofmann, and S. Whiteson. Varibad: A very good method for bayes-adaptive deep rl via meta-learning. *arXiv preprint arXiv:1910.08348*, 2019.

[13] V. Makoviychuk, L. Wawrzyniak, Y. Guo, M. Lu, K. Storey, M. Macklin, D. Hoeller, N. Rudin, A. Allshire, A. Handa, and G. State. Isaac gym: High performance gpu-based physics simulation for robot learning, 2021.

[14] R. Y. Rubinstein and D. P. Kroese. *The cross-entropy method: a unified approach to combinatorial optimization, Monte-Carlo simulation, and machine learning*, volume 133. Springer, 2004.

[15] D. Coleman, I. Sucan, S. Chitta, and N. Correll. Reducing the barrier to entry of complex robotic software: a moveit! case study. *arXiv preprint arXiv:1404.3785*, 2014.

[16] J.-M. Marin, P. Pudlo, C. P. Robert, and R. J. Ryder. Approximate bayesian computational methods. *Statistics and computing*, 22(6):1167–1180, 2012.

[17] M. Engel, O. Kanjilal, I. Papaioannou, and D. Straub. Bayesian updating and marginal likelihood estimation by cross entropy based importance sampling. *Journal of Computational Physics*, 473:111746, 2023.

[18] F. Ramos, R. C. Possas, and D. Fox. Bayessim: adaptive domain randomization via probabilistic inference for robotics simulators. *arXiv preprint arXiv:1906.01728*, 2019.

[19] N. Marlier, O. Brüls, and G. Louppe. Simulation-based bayesian inference for multi-fingered robotic grasping. *arXiv preprint arXiv:2109.14275*, 2021.

[20] S. Hochreiter and J. Schmidhuber. Long short-term memory. *Neural computation*, 9(8):1735–1780, 1997.

[21] K. Sohn, H. Lee, and X. Yan. Learning structured output representation using deep conditional generative models. *Advances in neural information processing systems*, 28, 2015.

[22] C. Finn, P. Abbeel, and S. Levine. Model-agnostic meta-learning for fast adaptation of deep networks. In *International conference on machine learning*, pages 1126–1135. PMLR, 2017.

[23] Y. Duan, J. Schulman, X. Chen, P. L. Bartlett, I. Sutskever, and P. Abbeel. Rl ˆ2: Fast reinforcement learning via slow reinforcement learning. *arXiv preprint arXiv:1611.02779*, 2016.

[24] Z. I. Botev, D. P. Kroese, R. Y. Rubinstein, and P. L'Ecuyer. The cross-entropy method for optimization. In *Handbook of statistics*, volume 31, pages 35–59. Elsevier, 2013.

[25] A. X. Chang, T. Funkhouser, L. Guibas, P. Hanrahan, Q. Huang, Z. Li, S. Savarese, M. Savva, S. Song, H. Su, et al. Shapenet: An information-rich 3d model repository. *arXiv preprint arXiv:1512.03012*, 2015.

[26] C. R. Qi, H. Su, K. Mo, and L. J. Guibas. Pointnet: Deep learning on point sets for 3d classification and segmentation. In *Proceedings of the IEEE conference on computer vision and pattern recognition*, pages 652–660, 2017.

[27] T. Daniel and A. Tamar. Soft-introvae: Analyzing and improving the introspective variational autoencoder. In *Proceedings of the IEEE/CVF Conference on Computer Vision and Pattern Recognition*, pages 4391–4400, 2021.

[28] H. Ren and P. Ben-Tzvi. Learning inverse kinematics and dynamics of a robotic manipulator using generative adversarial networks. *Robotics and Autonomous Systems*, 124:103386, 2020.

[29] C.-M. Hung, S. Zhong, W. Goodwin, O. P. Jones, M. Engelcke, I. Havoutis, and I. Posner. Reaching through latent space: From joint statistics to path planning in manipulation. *IEEE Robotics and Automation Letters*, 7(2):5334–5341, 2022.

[30] R. Bensadoun, S. Gur, N. Blau, T. Shenkar, and L. Wolf. Neural inverse kinematics, 2022.

[31] E. Coumans and Y. Bai. Pybullet, a python module for physics simulation for games, robotics and machine learning. 2016.

[32] J. Tobin, R. Fong, A. Ray, J. Schneider, W. Zaremba, and P. Abbeel. Domain randomization for transferring deep neural networks from simulation to the real world. In *2017 IEEE/RSJ international conference on intelligent robots and systems (IROS)*, pages 23–30. IEEE, 2017.

[33] A. Paszke, S. Gross, S. Chintala, G. Chanan, E. Yang, Z. DeVito, Z. Lin, A. Desmaison, L. Antiga, and A. Lerer. Automatic differentiation in pytorch. In *NIPS-W*, 2017.

[34] K. Rakelly, A. Zhou, C. Finn, S. Levine, and D. Quillen. Efficient off-policy meta-reinforcement learning via probabilistic context variables. In *International conference on machine learning*, pages 5331–5340. PMLR, 2019.

[35] D. P. Kingma and J. Ba. Adam: A method for stochastic optimization. *arXiv preprint arXiv:1412.6980*, 2014.

[36] J. Lundell, F. Verdoja, and V. Kyrki. Robust grasp planning over uncertain shape completions. In *2019 IEEE/RSJ International Conference on Intelligent Robots and Systems (IROS)*, pages 1526–1532. IEEE, 2019.

[37] S. Chen, X. Ma, Y. Lu, and D. Hsu. Ab initio particle-based object manipulation. *arXiv preprint arXiv:2107.08865*, 2021.

[38] Y. Sun, Y. Wang, Z. Liu, J. Siegel, and S. Sarma. Pointgrow: Autoregressively learned point cloud generation with self-attention. In *Proceedings of the IEEE/CVF Winter Conference on Applications of Computer Vision*, pages 61–70, 2020.

[39] L. Zhou, Y. Du, and J. Wu. 3d shape generation and completion through point-voxel diffusion. In *Proceedings of the IEEE/CVF International Conference on Computer Vision*, pages 5826–5835, 2021.

[40] Y. Cai, K.-Y. Lin, C. Zhang, Q. Wang, X. Wang, and H. Li. Learning a structured latent space for unsupervised point cloud completion. In *Proceedings of the IEEE/CVF Conference on Computer Vision and Pattern Recognition*, pages 5543–5553, 2022.